Potential and Field of a Homogeneous Magnetic Spheroid of Arbitrary Direction in a Homogeneous Magnetic Field in Cartesian Coordinates.

Markus Kraiger * Bernhard Schnizer †

January 2012, revised May 2012, published June 2013: COMPEL (The International Journal for Computation and Mathematics in Electrical and Electronic Engineering), v.23, 3, pp.936 to 960.
Manuscript corrected: 2014-01-14

1 Introduction

We derive expressions for the potential and the magnetic field of prolate and oblate spheroids with permeability μ_2 inserted into a static homogeneous magnetic field in a medium with permeability μ_1. Both directions, that of the primary field and that of the symmetry axis, are completely arbitrary. The potential and the field components as well as the arguments of these functions are expressed in Cartesian coordinates. Though the centre of the spheroid is at the origin, it is easy to change all the formulas for another position of the spheroidal centre. This grants more freedom, flexibility and ease for building complex structures composed of arbitrarily arranged spheroids.

Our derivations start from previous work (Kuchel and Bulliman, 1989) where the two problems have been solved for spheroids in prolate or oblate spheroidal coordinates with the z-axis as the symmetry axis and a homogeneous static external field of arbitrary direction. The potentials and the fields have also been expressed in Cartesian coordinates except for three functions in $\cosh\eta$ (in the prolate case) or in $\sinh\eta$ (in the oblate case), where η is the quasi-radial variable. We succeeded in replacing these hyperbolic functions by square root expressions involving Cartesian coordinates. These square roots depend on the square of the radius, a rotation invariant, and on z^2, which is invariant under rotations around the symmetry axis. All other terms of the potentials depend on similar invariants. These dependences permit one to go from the $z-$axis to an arbitrary vector as the symmetry axis. The gradients of the potentials are needed to determine the field expressions. For this purpose the gradients of

*Institute of Medical Engineering, Technische Universität Graz, Kronesgasse 5 , A-8010 Graz

†Inst. f. Theoretische Physik-Computational Physics, Technische Universität Graz, Petersgasse 16, A-8010 Graz

the three functions occuring in the potentials are computed and simplified. All these expressions are derived in the third and fourth section.

When deriving these potentials and fields we had in mind magnetic resonance imaging (MRI) and magnetic resonance spectroscopy (MRS). These make use of the Larmor resonance signals emitted by protons precessing in the local magnetic induction, which is excited by an external static magnetic field. In general, the MR signal is highly sensitive to the magnetic properties of the matter surrounding the nuclei. Theoretical studies of the resonance signal behaviour in situations of varying magnetic susceptibilities and dynamic physiological processes as for instance diffusion utilize the analytical magnetostatic solutions of specific geometrical bodies. Models of structures like cells or blood vessels can be built up from arrays of simple magnetic bodies. In particular prolate and oblate spheroids are used as such building blocks to analyse the local magnetic field distribution in the vicinity of blood cells in MRS of cells (Kuchel and Bulliman, 1989). The magnetic susceptibilities of biological matter are small. Hence the total field a proton experiences consists of the primary field and of the perturbation fields of all the spheroids used to model the structure under investigation. Since the magnetic susceptibilities of the biological materials are small the interaction between the various spheroids may be neglected. So the proposed approach described below gives a good approximation.

In this way a toolbox for MRI and MRS resonance signal analyses with flexible instruments is provided capable of modelling several biological tissues of interest such as trabecular bone, microvascular network and general interfaces of adjacent tissues. We give only a short survey of such applications in the fifth section. More detailed accounts of such investigations will be submitted to pertinent journals of medical physics.

Conclusions regarding the results obtained and listing of motivation and other applications are contained in the sixth section.

2 Primary and Total Field

The primary field is a homogeneous static magnetic field. In the general case this is written as

$$\begin{aligned} \mathbf{H}_0 &= (H_{0x}, H_{0y}, H_{0z}) \\ &= H_0\ (\sin\beta\ \cos\alpha,\ \sin\beta\ \sin\alpha,\ \cos\beta) \end{aligned} \tag{1}$$

with the corresponding potential

$$\Phi_0(x,y,z) = -\ (H_{0x}\ x\ +\ H_{0y}\ y\ +\ H_{0z}\ z) \tag{2}$$

A spheroid with magnetic permeability $\mu_2 = \mu_0(1+\chi_2)$ is surrounded by an infinite medium with magnetic permeability $\mu_1 = \mu_0(1+\chi_1)$. The total external field $\mathbf{H}_1$ and the corresponding potential Φ_1 must assume the asymptotic values

$$\lim_{|\mathbf{r}|\to\infty} \mathbf{H}_1 = \mathbf{H}_0, \qquad \lim_{|\mathbf{r}|\to\infty} \Phi_1 = \Phi_0. \tag{3}$$

The presence of the spheroid induces perturbation fields in the exterior and the interior, with potentials Φ_{1r} and Φ_{2r}. The corresponding total fields, $\Phi_1 =$

$\Phi_{1r} + \Phi_0$ and $\Phi_2 = \Phi_{2r} + \Phi_0$ must fulfil the following two continuity conditions at the surface of the spheroid:

$$\mathbf{r} = \mathbf{r}_s : \quad \Phi_1 = \Phi_2, \quad \mu_1 \ (\mathbf{s} \cdot \nabla \Phi_1)\Big|_{\mathbf{r}=\mathbf{r}_s} = \mu_2 \ (\mathbf{s} \cdot \nabla \Phi_2)\Big|_{\mathbf{r}=\mathbf{r}_s}. \tag{4}$$

$\mathbf{s}$ is the normal to the surface of the spheroid. All these conditions define a unique solution to be found in the next chapters for prolate and oblate spheroids.

3 A Prolate Spheroid in a Homogeneous Magnetic Field

For a prolate spheroid (semi-axes a_p, a_p, c_p; $c_p > a_p$) with magnetic permeability μ_2 in a medium with magnetic permeability μ_1 and in an external homogeneous field (1) the boundary value problem has been solved in prolate spheroidal coordinates (Kuchel and Bulliman, 1989). The symmetry axis is the z-axis. The direction of the primary field is arbitrary (cf. eq.(1)). We repeat just the essential equations of this reference. Then we use these expressions to go over to Cartesian coordinates. Finally these expressions are generalized to the case where both the symmetry axis and that of the primary field are completely arbitrary.

3.1 The reaction field in prolate spheroidal coordinates

At first the boundary value problem is solved in prolate spheroidal coordinates (s., for example, (Moon and Spencer, 1988), Fig.1.06).

$$x = e_p \ \sinh\eta \ \sin\theta \ \cos\psi, \tag{5}$$
$$y = e_p \ \sinh\eta \ \sin\theta \ \sin\psi, \tag{6}$$
$$z = e_p \ \cosh\eta \ \cos\theta; \tag{7}$$
$$e_p = \sqrt{c_p^2 - a_p^2} \tag{8}$$

for a spheroid, whose symmetry axis coincides with the z-axis. The potential equation can be solved by separation.

$$\Phi(\eta, \theta, \psi) \ = \ H(\eta) \ \Theta(\theta) \ \Psi(\psi). \tag{9}$$

The particular solutions of the resulting ordinary differential equation for the quasi-radial functions $H(\eta)$ are Legendre polynomials or functions in $\cosh\eta$. The solutions $\Theta(\theta)$ must be Legendre polynomials in $\cos\theta$; Legendre functions in $\cos\theta$ are singular at $\theta = 0, \pi$; so they must be excluded. In each term the order n of the quasi-radial functions must agree with that of the Legendre polynomial $P_n^m(\cos\theta)$. $\Psi(\psi)$ are the trigonometric functions $\cos(m\psi)$ or $\sin(m\psi)$.

The interface separating the two domains is the spheroid:

$$\frac{x^2}{a_p^2} + \frac{y^2}{a_p^2} + \frac{z^2}{c_p^2} = 1 \quad \Leftrightarrow \quad \eta = \eta_p = \mathrm{Arcoth}(c_p/a_p). \tag{10}$$

One starts inserting the spheroidal coordinates into the primary potential (2). Thereafter these are replaced by the corresponding particular solutions of

the potential equation using

$$P_1^0(\cos\theta) = \cos\theta,\ P_1^1(\cos\theta) = \sin\theta; \quad P_1^0(\cosh\eta) = \cosh\eta,\ P_1^1(\cosh\eta) = \sinh\eta \tag{11}$$

to give:

$$\begin{aligned} \Phi_0 \quad = \quad & -\, e_p\ P_1^1(\cosh\eta)\ P_1^1(\cos\theta)\ (H_{0x}\cos\psi + H_{0y}\sin\psi) \\ & -\, e_p\ P_1^0(\cosh\eta)\ P_1^0(\cos\theta)\ H_{0z}. \end{aligned} \tag{12}$$

The perturbation field in the exterior must vanish at infinity. This is ensured by the Legendre functions of the quasi-radial variable in the following series expansions:

$$\begin{aligned} & \eta \geq \eta_p : \\ & \qquad \Phi_{1r} \quad = \quad \sum_{m=0}^{1} {}_1A_1^m\ Q_1^m(\cosh\eta) P_1^m(\cos\theta)\cos(m\psi)\ + \\ & \qquad\qquad\qquad + {}_1B_1^1\ Q_1^1(\cosh\eta) P_1^1(\cos\theta)\sin(m\psi). \end{aligned} \tag{13}$$

In the interior the total field must be finite at the origin. This excludes the Legendre functions for the quasi-radial variable.

$$\begin{aligned} & \eta \leq \eta_p : \\ & \qquad \Phi_2 \quad = \quad \sum_{m=0}^{1} {}_2A_1^m\ P_1^m(\cosh\eta) P_1^m(\cos\theta)\cos(m\psi)\ + \\ & \qquad\qquad\qquad + \quad {}_2B_1^1\ P_1^1(\cosh\eta) P_1^1(\cos\theta)\sin(m\psi). \end{aligned} \tag{14}$$

These sums are inserted into the two continuity conditions (4). The normal derivative $\mathbf{s}\cdot\nabla$ becomes just the derivation $\partial/\partial\eta$ up to a metric coefficient, which cancels on both sides of the equation. In view of the orthogonality of the Legendre polynomials $P_n^m(\cos\theta)$ and of the trigonometric functions these two conditions involving sums are decomposed into three system of two linear equations for the expansion coefficients. Each system comprises just a single pair of the parameters n and m. Solving these systems gives the expansion coefficients listed below.

One may start with a more general expansion comprising infinite sums in n and m. One inserts these infinite sums into the two continuity conditions (4). The aforementioned orthogonality leads to an infinite system of pairs of linear equations. But for $n \neq 1$ and $m \neq 0$ nor $\neq 1$ these systems are linear homogeneous equations for the unknown coefficients ${}_2A_n^m, {}_2B_n^m, {}_1A_n^m$ and ${}_1B_n^m$ giving zero solutions. So the simple approach as well as the more complicated

one give the same solutions:

$$
\begin{aligned}
{}_1A_1^0 &= \frac{e_p\ H_{0z}\ (\mu_2-\mu_1)\ P_1^0\ P_1^{0'}}{\mu_2\ P_1^{0'}\ Q_1^0\ -\ \mu_1\ P_1^0\ Q_1^{0'}} \\
&:= e_p\ H_{0z}\ L_0, \qquad (15)\\
{}_2A_1^0 &= e_p\ H_{0z}\ \mu_1\ \left(\frac{P_1^{0'}\ Q_1^0\ -\ P_1^0\ Q_1^{0'}}{\mu_1\ P_1^0\ Q_1^{0'}\ -\ \mu_2\ P_1^{0'}\ Q_1^0}\right) \\
&:= e_p\ H_{0z}\ M_0; \qquad (16)\\
{}_1A_1^1 &= \frac{e_p H_{0x}\ (\mu_2-\mu_1)\ P_1^1\ P_1^{1'}}{\mu_2\ P_1^{1'}\ Q_1^1\ -\ \mu_1\ P_1^1\ Q_1^{1'}} \\
&:= e_p\ H_{0x}\ L_1, \qquad (17)\\
{}_1B_1^1 &= e_p\ H_{0y}\ L_1, \qquad (18)\\
{}_2A_1^1 &= e_p\ H_{0x}\ \mu_1\ \left(\frac{P_1^{1'}\ Q_1^1\ -\ P_1^1\ Q_1^{1'}}{\mu_1\ P_1^1\ Q_1^{1'}\ -\ \mu_2\ P_1^{1'}\ Q_1^1}\right) \\
&:= e_p\ H_{0x}\ M_1, \qquad (19)\\
{}_2B_1^1 &= e_p\ H_{0y}\ M_1. \qquad (20)
\end{aligned}
$$

The argument of all the Legendre polynomials and functions in the above equations is $\cosh\eta_p$. The solutions have been obtained with the help of *Mathematica*. The corresponding notebook named ProlateCoefficients.nb can be found at a website (Kraiger and Schnizer, 2011). The solutions agree with those of (Kuchel and Bulliman, 1989). In the same reference it has been shown that the Legendre functions and polynomials may be replaced with elementary functions

$$
\begin{aligned}
Q_1^0(\cosh\eta) &= \cosh\eta\ \mathrm{Arcoth}(\cosh\eta) - 1, \\
Q_1^1(\cosh\eta) &= \sinh\eta\ \mathrm{Arcoth}(\cosh\eta) - \coth\eta. \qquad (21)
\end{aligned}
$$

The above results are inserted into eq.(14); the total interior potential comes out as that of a homogeneous field:

$$
\begin{aligned}
&\eta \le \eta_p : \\
&\quad \Phi_2 = e_p\ M_1\ (H_{0x}\ \cos\psi + H_{0y}\sin\psi)\ \sinh\eta\ \sin\theta \\
&\qquad + e_p\ M_0\ H_{0z}\ \cosh\eta\ \cos\theta. \\
&\Phi_2(x,y,z) = M_1\ (H_{0x}\ x\ +\ H_{0y}\ y)\ + M_0\ H_{0z}\ \ z. \qquad (22)
\end{aligned}
$$

Similarly one gets for the exterior reaction field:

$$
\begin{aligned}
&\eta \ge \eta_p : \\
&\quad \Phi_{r1} = e_p\ (H_{0x}\ \cos\psi + H_{0y}\sin\psi)\times \qquad (23)\\
&\qquad \times\ L_1\ (\sinh\eta\ \mathrm{Arcoth}(\cosh\eta) - \coth\eta)\sin\theta \\
&\qquad + e_p\ H_{0z}\ L_0\ \ (\cosh\eta\ \mathrm{Arcoth}(\cosh\eta) - 1)\cos\theta\ , \\
&\qquad = L_1\ \big(H_{0x}\ x\ +\ H_{0y}\ y\big)\big(f_1(\eta)\ -\ f_2(\eta)\big)\ +\ L_0\ H_{0z}\ z\ \big(f_1(\eta) - f_3(\eta)\big),
\end{aligned}
$$

with

$$f_1(\eta) = \mathrm{Arcoth}(\cosh\eta), \tag{24}$$

$$f_2(\eta) = \frac{\cosh\eta}{\sinh^2\eta}, \tag{25}$$

$$f_3(\eta) = \frac{1}{\cosh\eta}. \tag{26}$$

The functions $f_1(\eta), f_2(\eta), f_3(\eta)$ above depend solely on the quasi-radial variable $\cosh\eta$. In the exterior of the spheroid is $\eta \geq \eta_p > 1$; so the three functions just introduced are well-defined, real, finite and non-zero in the exterior of the spheroid.

Inserting the substitutions (11), (21) and their derivatives into the definitions of the constants L_0, L_1, M_0, M_1 above and going over to the susceptibilities the expressions for these constants become after some algebra:

$$L_0 = \frac{(\chi_1 - \chi_2)\cosh\eta_p}{1 + \chi_2 - (1+\chi_1)\coth^2\eta_p + (\chi_1 - \chi_2)\cosh(\eta_p)\mathrm{Arcoth}(\cosh\eta_p)}, \tag{27}$$

$$L_1 = \frac{\chi_1 - \chi_2}{(2 + \chi_1 + \chi_2)\ \mathrm{csch}^2\eta_p\ \mathrm{sech}\eta_p\ +\ (\chi_1 - \chi_2)\big(\mathrm{Arcoth}(\cosh\eta_p) - \mathrm{sech}\eta_p\big)}, \tag{28}$$

$$M_0 = -\frac{1\ +\ \chi_1}{1 + \chi_1\ +\ (\chi_1 - \chi_2)\sinh^2\eta_p\,(1 - \cosh\eta_p\ \mathrm{Arcoth}(\cosh\eta_p))}, \tag{29}$$

$$M_1 = -\frac{2\ (1\ +\ \chi_1)}{(2 + \chi_1 + \chi_2)\ -\ (\chi_1 - \chi_2)\sinh^2\eta_p\,(1 - \cosh\eta_p\ \mathrm{Arcoth}(\cosh\eta_p))}. \tag{30}$$

If both media are the same the above coefficients become:

$$\chi_2 \to \chi_1: \quad L_0 \to 0,\ L_1 \to 0,\ M_0 \to -1,\ M_1 \to -1. \tag{31}$$

The exterior reaction potential, eq.(23), then assumes the value zero. The total interior potential, eq.(22), becomes equal to the primary potential, eq.(2). So the interior reaction potential is:

$$\begin{aligned} \Phi_{2r}(x,y,z) &= \Phi_2(x,y,z)\ -\ \Phi_0(x,y,z) = \\ &= \big(H_{0x}\ x\ +\ H_{0y}\ y\big)(M_1 + 1)\ +\ H_{0z}\ z\ (M_0 + 1). \end{aligned} \tag{32}$$

3.2 The reaction field in Cartesian coordinates

We want expressions for the potential which depend on x, y, z only. So $\cosh\eta$ must be replaced with a corresponding expression in Cartesian coordinates. From eqs.(5) to (7) one finds:

$$\cosh^2\eta = \frac{1}{2}\left(1 + \frac{r^2}{e_p^2} \pm \sqrt{\left(1 + \frac{r^2}{e_p^2}\right)^2 - 4\frac{z^2}{e_p^2}}\right).$$

Intense numerical studies show that only the plus sign applies. So we have:

$$\cosh\eta \;=\; \frac{1}{\sqrt{2}}\sqrt{1+\frac{r^2}{e_p^2}+w_p(\mathbf{r},\mathbf{e}_z)} \;:=\; u_p(\mathbf{r},\mathbf{e}_z)/\sqrt{2}, \tag{33}$$

$$w_p(\mathbf{r},\mathbf{e}_z) \;=\; \sqrt{\left(1+\frac{r^2}{e_p^2}\right)^2-4\frac{z^2}{e_p^2}} \;=\; \sqrt{\left(1+\frac{r^2}{e_p^2}\right)^2-4\frac{(\mathbf{e}_z\cdot\mathbf{r})^2}{e_p^2}}, \tag{34}$$

$$r^2 \;=\; x^2+y^2+z^2. \tag{35}$$

Inserting this expression for $\cosh\eta$ into eqs.(24) to (26)

$$f_1(\mathbf{r},\mathbf{e}_z) \;=\; \mathrm{Arcoth}(u_p(\mathbf{r},\mathbf{e}_z)/\sqrt{2}), \tag{36}$$

$$f_2(\mathbf{r},\mathbf{e}_z) \;=\; \frac{\sqrt{2}\;u_p(\mathbf{r},\mathbf{e}_z)}{u_p(\mathbf{r},\mathbf{e}_z)^2-2}, \tag{37}$$

$$f_3(\mathbf{r},\mathbf{e}_z) \;=\; \frac{\sqrt{2}}{u_p(\mathbf{r},\mathbf{e}_z)}. \tag{38}$$

and inserting the resulting expressions for f_1, f_2, f_3 into eq.(23) we get the final expression for the exterior potential as a pure function of the Cartesian coordinates x, y, z:

$$\begin{aligned}\Phi_{r1}(x,y,z) \;=\;& L_1\;(H_{0x}\;x\;+H_{0y}\;y)\;\big(f_1(\mathbf{r},\mathbf{e}_z)\;-f_2(\mathbf{r},\mathbf{e}_z)\big)\;+\\ &+\;L_0\;H_{0z}\;z\;\big(f_1(\mathbf{r},\mathbf{e}_z)\;-\;f_3(\mathbf{r},\mathbf{e}_z)\big).\end{aligned} \tag{39}$$

As stated after eqs.(26) these functions encounter no problems in the exterior of the spheroid. The interior potential, eq.(32), is already a simple function of the Cartesian coordinates.

3.3 Potential and field for an arbitrary direction of the spheroidal symmetry axis

For applications it is necessary to consider spheroids whose symmetry axis has an arbitrary direction. The corresponding expressions for the potential will be derived from those given in eqs.(39) and (32). These are rewritten in a way suggesting a general form:

$$\begin{aligned}\Phi_{r1}(x,y,z) \;=\;& (\mathbf{H}_{0\perp}\cdot\mathbf{r}_\perp)\;L_1\;(f_1(\mathbf{r},\mathbf{e}_z)-f_2(\mathbf{r},\mathbf{e}_z))\;+\\ &+\;(\mathbf{H}_{0\parallel}\cdot\mathbf{r}_\parallel)\;L_0\;(f_1(\mathbf{r},\mathbf{e}_z)-f_3(\mathbf{r},\mathbf{e}_z)),\\ \Phi_{r2}(x,y,z) \;=\;& (\mathbf{H}_{0\perp}\cdot\mathbf{r}_\perp)\;(M_1+1)\;+\;(\mathbf{H}_{0\parallel}\cdot\mathbf{r}_\parallel)(M_0+1).\end{aligned} \tag{40}$$

The vectors $\mathbf{H}_{0\parallel}, \mathbf{r}_\parallel$ give the projections of the corresponding vector parallel to the symmetry axis, i.e. the z-axis. Similarly, the vectors $\mathbf{H}_{0\perp} = (H_{0x}, H_{0y}, 0)$, $\mathbf{r}_\perp = (x, y, 0)$ give the vector corresponding to the projection onto the x,y-plane, which is perpendicular to the symmetry axis.

Now it is easy to accomplish the substitutions for an arbitrary direction of the symmetry axis given by the unit vector $\mathbf{n}$. Any vector $\mathbf{s}$ may be decomposed into a component parallel to $\mathbf{n}$ and one perpendicular to that vector:

$$\mathbf{s} \;=\; \mathbf{s}_\parallel \;+\; \mathbf{s}_\perp \;=\; \mathbf{n}(\mathbf{s}\cdot\mathbf{n}) \;+\; \big(\mathbf{s} \;-\; \mathbf{n}(\mathbf{s}\cdot\mathbf{n})\big). \tag{41}$$

In $w_p(\mathbf{r},\mathbf{e}_z)$, eq.(34), only the variable $z = (\mathbf{e}_z \cdot \mathbf{r})$, the component of the position vector along $\mathbf{e}_z$, must be replaced by $(\mathbf{n} \cdot \mathbf{r})$ giving:

$$\cosh\eta = \frac{1}{\sqrt{2}}\sqrt{1+\frac{r^2}{e_p^2}+w_p(\mathbf{r},\mathbf{n})} := u_p(\mathbf{r},\mathbf{n})/\sqrt{2}, \tag{42}$$

$$w_p(\mathbf{r},\mathbf{n}) = \sqrt{\left(1+\frac{r^2}{e_p^2}\right)^2 - 4\frac{(\mathbf{n}\cdot\mathbf{r})^2}{e_p^2}}. \tag{43}$$

The functions f_i, eqs.(36) to (38), remain the same except that $u_p(\mathbf{r},\mathbf{e}_z)$ and $w_p(\mathbf{r},\mathbf{e}_z)$ must be replaced with $u_p(\mathbf{r},\mathbf{n})$ and $w_p(\mathbf{r},\mathbf{n})$ giving the new functions $f_i(\mathbf{r},\mathbf{n})$:

$$f_1(\mathbf{r},\mathbf{n}) = \mathrm{Arcoth}(u_p(\mathbf{r},\mathbf{n})/\sqrt{2}), \tag{44}$$

$$f_2(\mathbf{r},\mathbf{n}) = \frac{\sqrt{2}\ u_p(\mathbf{r},\mathbf{n})}{\left(u_p(\mathbf{r},\mathbf{n})\right)^2-2}, \tag{45}$$

$$f_3(\mathbf{r},\mathbf{n}) = \frac{\sqrt{2}}{u_p(\mathbf{r},\mathbf{n})}. \tag{46}$$

Inserting all these new functions into eqs.(40) gives the potential for a prolate spheroid whose symmetry axis is given by the arbitrary unit vector $\mathbf{n}$:

$$\begin{aligned}\Phi_{r1}(x,y,z) &= L_1\ (\mathbf{H}_0\cdot\mathbf{r})\ \big(f_1(\mathbf{r},\mathbf{n})\ -\ f_2(\mathbf{r},\mathbf{n})\big)\ + \\ &+\ (\mathbf{H}_0\cdot\mathbf{n})(\mathbf{n}\cdot\mathbf{r})\ \big[\ L_0\ \big(f_1(\mathbf{r},\mathbf{n})\ -\ f_3(\mathbf{r},\mathbf{n})\big)\ - \\ &\qquad -\ L_1\ \big(f_1(\mathbf{r},\mathbf{n})\ -\ f_2(\mathbf{r},\mathbf{n})\big)\big],\end{aligned} \tag{47}$$

$$\Phi_{r2}(x,y,z) = (\mathbf{H}_0\cdot\mathbf{r})\ (M_1+1)\ +\ (\mathbf{H}_0\cdot\mathbf{n})(\mathbf{n}\cdot\mathbf{r})\ [M_0\ -\ M_1]. \tag{48}$$

The evaluation of the magnetic field requires the gradients of the functions $f_i(\mathbf{r},\mathbf{n})$. These are done by symbolic computation. Since the resulting expressions consist again of polynomials and the square roots already occuring in the potential it is possible to find simpler expressions. These are again checked against the original gradients by symbolic computation. All gradients are proportional to the vector $\mathbf{r}_p$:

$$\mathbf{r}_p := \frac{\sqrt{2}}{e_p^2}\left(\mathbf{r} - 2\mathbf{n}\ \frac{(\mathbf{n}\cdot\mathbf{r})}{[u_p(\mathbf{r},\mathbf{n})]^2}\right). \tag{49}$$

$$\nabla f_1(\mathbf{r},\mathbf{n}) - \nabla f_2(\mathbf{r},\mathbf{n}) = \frac{u_p(\mathbf{r},\mathbf{n})}{w_p(\mathbf{r},\mathbf{n})}\ \frac{4}{[(u_p(\mathbf{r},\mathbf{n}))^2-2]^2}\ \mathbf{r}_p, \tag{50}$$

$$\nabla f_1(\mathbf{r},\mathbf{n}) - \nabla f_3(\mathbf{r},\mathbf{n}) = \frac{2}{[2-(u_p(\mathbf{r},\mathbf{n}))^2]\ u_p(\mathbf{r},\mathbf{n})\ w_p(\mathbf{r},\mathbf{n})}\ \mathbf{r}_p. \tag{51}$$

The corresponding checks are contained in the notebook ProlatePotDerivatives.nb (Kraiger and Schnizer, 2011).

The vector $\mathbf{r}_p$ and all the gradients listed above are well-defined and real in the exterior of the spheroid, including the interface, where $\eta \geq \eta_p$, which

is equivalent with the condition (55) in Cartesian coordinates. In fact, a more detailed analysis shows that on the interface:

$$u_p(\mathbf{r},\mathbf{n}) = \sqrt{2}\ \cosh\eta_p, \tag{52}$$

$$w_p(\mathbf{r},\mathbf{n}) = \sqrt{z^4/\big(e_p\ \cosh(\eta_p)\big)^4\ -\ 2z^2/e_p^2\ +\ \cosh^4\eta_p} \tag{53}$$

$$\sinh^2\eta_p \le w_p(\mathbf{r},\mathbf{n}) \le \cosh^2\eta_p. \tag{54}$$

For example, for a = 1, c = 2, ($e_p = \sqrt{3}$) one finds $\sqrt{2}\ \cosh\eta_p = 2\sqrt{2/3} = 1.63... > \sqrt{2}$; $1/3 \le w_p(\mathbf{r},\mathbf{n}) \le 4/3$.

3.4 Final formulas for the field

So the final formulas for the reaction field excited in an arbitray homogeneous primary field $\mathbf{H}_0$ by a prolate spheroid with arbitrary symmetry axis given by a unit vector $\mathbf{n}$ is in the exterior:

$$\frac{r^2-(\mathbf{n}\cdot\mathbf{r})^2}{a_p^2} + \frac{(\mathbf{n}\cdot\mathbf{r})^2}{c_p^2} \ge 1\ : \tag{55}$$

$$\begin{aligned}
\mathbf{H}_{r1}(x,y,z) = &-\mathbf{H}_0\ L_1\ \big(f_1(\mathbf{r},\mathbf{n}) - f_2(\mathbf{r},\mathbf{n})\big)\ - \\
&-\mathbf{n}(\mathbf{H}_0\cdot\mathbf{n})\big[L_0\ \big(f_1(\mathbf{r},\mathbf{n}) - f_3(\mathbf{r},\mathbf{n})\big)\ -\ L_1\ \big(f_1(\mathbf{r},\mathbf{n}) - f_2(\mathbf{r},\mathbf{n})\big)\big] \\
&-\mathbf{r}_p\ (\mathbf{H}_0\cdot\mathbf{r})\ L_1\ \frac{u_p(\mathbf{r},\mathbf{n})}{w_p(\mathbf{r},\mathbf{n})}\ \frac{4}{[(u_p(\mathbf{r},\mathbf{n}))^2-2]^2} \\
&-\mathbf{r}_p\ (\mathbf{H}_0\cdot\mathbf{n})(\mathbf{r}\cdot\mathbf{n})\ L_0\ \frac{2}{[2-(u_p(\mathbf{r},\mathbf{n}))^2]u_p(\mathbf{r},\mathbf{n})\ w_p(\mathbf{r},\mathbf{n})} \\
&+\mathbf{r}_p\ (\mathbf{H}_0\cdot\mathbf{n})(\mathbf{r}\cdot\mathbf{n})\ L_1\ \frac{4\ u_p(\mathbf{r},\mathbf{n})}{w_p(\mathbf{r},\mathbf{n})\ [(u_p(\mathbf{r},\mathbf{n}))^2-2]^2};
\end{aligned} \tag{56}$$

and in the interior:

$$\frac{r^2-(\mathbf{n}\cdot\mathbf{r})^2}{a_p^2} + \frac{(\mathbf{n}\cdot\mathbf{r})^2}{c_p^2} \le 1\ :$$

$$\mathbf{H}_{r2}(x,y,z) = -\mathbf{H}_0\ (M_1+1)\ -\ \mathbf{n}\ (\mathbf{H}_0\cdot\mathbf{n})\ [M_0\ -\ M_1]. \tag{57}$$

3.5 Concluding remarks for the field of the prolate spheroid

A prolate spheroid is inserted into an external homogeneous magnetic field $\mathbf{H}_0$ of arbitrary direction. Its permeability is $\mu_2 = \mu_0(1+\chi_2)$; while that of the surrounding medium is $\mu_1 = \mu_0(1+\chi_1)$. The spheroid has semi-axes $a_p, a_p, c_p,\ c_p > a_p$; these determine the excentricy e_p and the quasi-radial parameter η_p, eqs.(8) and (10). These in turn determine the coefficients L_0, L_1, M_0, M_1, eqs.(27) to (30). The spheroid's symmetry axis is the arbitrary unit vector $\mathbf{n}$. The reaction field due to the presence of the spheroid in the external field is given in Cartesian coordinates, $\mathbf{r} = (x,y,z)$, by eq.(56) in the exterior, by eq.(57) in the interior. The functions $f_1(\mathbf{r},\mathbf{n}), f_2(\mathbf{r},\mathbf{n}), f_3(\mathbf{r},\mathbf{n})$, eqs.(44) to (46), depend on the variables $u_p(\mathbf{r},\mathbf{n})$ and $w_p(\mathbf{r},\mathbf{n})$, eqs.(42) and (43). The needed gradients of the $f_i(\mathbf{r},\mathbf{n})$ are given in eqs.(50) and (51) . Eqs.(56) and eq.(57) are for a spheroid, whose centre is at the origin. If the centre is at the point $\mathbf{r}_0 = (x_0,y_0,z_0)$ then the vector $\mathbf{r}$ must replaced simply with $\mathbf{r}-\mathbf{r}_0$.

4 A Single Oblate Spheroid in a Homogeneous Magnetic Field

An oblate spheroid (semi-axes $a_o, a_o, c_o;\ c_o < a_o$) with magnetic permeability $\mu_2 = \mu_0(1+\chi_2)$ is in a medium with magnetic permeability $\mu_1 = \mu_0(1+\chi_1)$ and in an external field (1). The solution of this boundary value problem has been sketched in (Kuchel and Bulliman, 1989). We use a notation for the coefficients which differs somewhat from that employed in this reference. The derivations are quite analogous to those performed in the previous chapter. The main difference is the different analytical form of the quasi-radial particular solutions.

4.1 The reaction field in oblate spheroidal coordinates

The spheroid induces a reaction field represented by the potentials $\Phi_{r1}(x,y,z)$ in the exterior, by $\Phi_{r2}(x,y,z)$ in the interior. This problem has been solved in (Kuchel and Bulliman, 1989) in oblate spheroidal coordinates (s., for example, (Moon and Spencer, 1988), Fig.1.07).

$$\begin{aligned} x &= e_o\ \cosh\eta\ \sin\theta\ \cos\psi, && (58)\\ y &= e_o\ \cosh\eta\ \sin\theta\ \sin\psi, && (59)\\ z &= e_o\ \sinh\eta\ \cos\theta; && (60)\\ e_o &= \sqrt{a_o^2 - c_o^2} && (61) \end{aligned}$$

for a spheroid, whose symmetry axis coincides with the z-axis. $\Phi_0,\ \Phi_1 = \Phi_0 + \Phi_{r1},\ \Phi_2 = \Phi_0 + \Phi_{r2}$ must be solutions of the potential equation in oblate coordinates. This partial differential equation can be solved by separation. The particular solutions of the separated equations suitable for the problem under investigation are Legendre polynomials or functions in $i\sinh\eta$; Legendre polynomials in $\cos\theta$; trigonometric functions in ψ.

The interface separating the two domains is the spheroid:

$$\frac{x^2}{a_o^2} + \frac{y^2}{a_o^2} + \frac{z^2}{c_o^2} = 1 \quad \Leftrightarrow \quad \eta = \eta_o = \mathrm{Artanh}(c_o/a_o). \qquad (62)$$

The potential and the normal component of the magnetic induction must be continuous across this interface. So conditions (4) apply again.

One starts with expansion in the particular solutions fulfilling the boundary conditions. We already know from the previous chapter that only the parameter values n = 1, m = 0 and 1 are needed. We want to get real expansion coefficients. According to (Kuchel and Bulliman, 1989), eqs.(A64), the $P_1^m(i\sinh\eta)$ are purely imaginary, the $Q_1^m(i\sinh\eta)$ are real:

$$\begin{aligned} P_1^0(i\sinh\eta) &= i\sinh\eta, \\ P_1^1(i\sinh\eta) &= i\cosh\eta; && (63)\\ Q_1^0(i\sinh\eta) &= \sinh\eta\ \mathrm{arccot}(\sinh\eta)\ -\ 1, \\ Q_1^1(i\sinh\eta) &= \cosh\eta\ \mathrm{arccot}(\sinh\eta)\ -\ \tanh\eta. && (64) \end{aligned}$$

These reality properties are taken into account below by inserting imaginary units in the expansions for the potentials. The primary potential is expressed

as:

$$\begin{aligned}\Phi_0 &= i\ e_o\ H_{0z}\ P_1^0(i\sinh\eta)\ P_1^0(\cos\theta)\ - \\ &- i\ e_o\ (H_{0x}\ \cos\psi + H_{0y}\ \sin\psi)\ P_1^1(i\sinh\eta)\ P_1^1(\cos\theta) \qquad (65)\end{aligned}$$

by eqs.(58) to (60) and (63). The total potentials are assumed as:

$\eta \geq \eta_o$:

$$\begin{aligned}\Phi_1 &= \Phi_0 + \sum_{m=0}^{1} {}_1A_1^m\ Q_1^m(i\ \sinh\eta)P_1^m(\cos\theta)\cos(m\psi)\ + \\ &+ {}_1B_1^1\ Q_1^1(i\ \sinh\eta)P_1^1(\cos\theta)\sin\psi\ ; \qquad (66)\end{aligned}$$

$\eta \leq \eta_o$:

$$\begin{aligned}\Phi_2 &= \sum_{m=0}^{1} i\ {}_2A_1^m\ P_1^m(i\sinh\eta)P_1^m(\cos\theta)\cos(m\psi)\ + \\ &+ i\ {}_2B_1^1\ P_1^1(i\sinh\eta)P_1^1(\cos\theta)\sin\psi\ . \qquad (67)\end{aligned}$$

The sums are inserted into the continuity conditions (4). In view of the orthogonality of the Legendre polynomials $P_n^m(\cos\theta)$ and of the trigonometric functions these two conditions involving sums are decomposed into three independent systems with the solutions:

$$\begin{aligned}{}_1A_1^0 &= i\ \frac{e_o\ H_{0z}\ (\mu_2-\mu_1)\ P_1^0\ P_1^{0'}}{\mu_2\ P_1^{0'}\ Q_1^0\ -\ \mu_1\ P_1^0\ Q_1^{0'}} \\ &:= e_o\ H_{0z}\ \bar{L}_0, \qquad (68)\\ {}_2A_1^0 &= e_o\ H_{0z}\ \mu_1\ \left(\frac{P_1^{0'}\ Q_1^0\ -\ P_1^0\ Q_1^{0'}}{\mu_2\ P_1^{0'}\ Q_1^0\ -\ \mu_1\ P_1^0\ Q_1^{0'}}\right) \\ &:= e_o\ H_{0z}\ \bar{M}_0; \qquad (69)\\ {}_1A_1^1 &= i\ \frac{e_o\ H_{0x}\ (\mu_1-\mu_2)\ P_1^1\ P_1^{1'}}{\mu_2\ P_1^{1'}\ Q_1^1\ -\ \mu_1\ P_1^1\ Q_1^{1'}} \\ &:= e_o\ H_{0x}\ \bar{L}_1\ , \qquad (70)\\ {}_1B_1^1 &= e_o\ H_{0y}\ \bar{L}_1, \qquad (71)\\ {}_2A_1^1 &= e_o\ H_{0x}\ \mu_1\ \left(\frac{P_1^{1'}\ Q_1^1\ -\ P_1^1\ Q_1^{1'}}{\mu_2\ P_1^{1'}\ Q_1^1\ -\ \mu_1\ P_1^1\ Q_1^{1'}}\right) \\ &:= e_o\ H_{0x}\ \bar{M}_1\ , \qquad (72)\\ {}_2B_1^1 &= e_o\ H_{0y}\ \bar{M}_1\ . \qquad (73)\end{aligned}$$

The solutions are given in the notebook OblateCoefficients.nb (Kraiger and Schnizer, 2011). The argument of all the Lengendre polynomials and functions in all of the above equations is $i\sinh\eta_o$. Inserting these solutions and thereafter the elementary functions (63) and (64) we get the total interior potential as that of a homogeneous field:

$\eta \leq \eta_o$:

$$\begin{aligned}\Phi_2 &= -\ e_o\ \bar{M}_1\ (H_{0x}\ \cos\psi + H_{0y}\ \sin\psi)\ \cosh\eta\ \sin\theta - \\ &- e_o\ \bar{M}_0\ H_{0z}\ \sinh\eta\ \cos\theta. \\ \Phi_2(x,y,z) &= -\ \bar{M}_1\ (H_{0x}\ x\ + H_{0y}\ y)\ -\ H_{0z}\ z. \qquad (74)\end{aligned}$$

Similarly we get for the external reaction field:

$$\begin{aligned}
&\eta \geq \eta_o : \\
&\quad \Phi_{r1} \;=\; e_o\,(H_{0x}\;\cos\psi + H_{0y}\;\sin\psi)\times \\
&\qquad \times\,\bar{L}_1\,(\cosh\eta\,\operatorname{arccot}(\sinh\eta) - \tanh\eta)\sin\theta \\
&\qquad +\,e_o\;H_{0z}\;\bar{L}_0\;\;(\sinh\eta\,\operatorname{arccot}(\sinh\eta) - 1)\cos\theta\;, \\
&\qquad =\; -\,\bar{L}_1\;(H_{0x}\;x\;+H_{0y}\;y)(g_1(\eta) - g_2(\eta))\;\;-\;\;\bar{L}_0\;H_{0z}\;z\;(g_1(\eta) - g_3(\eta)).
\end{aligned} \tag{75}$$

The functions g_1, g_2, g_3 depend solely on the function $\sinh\eta$:

$$g_1(\eta) \;=\; \operatorname{arccot}(\sinh\eta), \tag{76}$$

$$g_2(\eta) \;=\; \frac{\sinh\eta}{\cosh^2\eta} \;=\; \frac{\sinh\eta}{1+\sinh^2\eta}, \tag{77}$$

$$g_3(\eta) \;=\; \frac{1}{\sinh\eta}. \tag{78}$$

Substituting eqs.(63) and (64) and their derivatives into the definitions of the constants $\bar{L}_0, \bar{L}_1, \bar{M}_0, \bar{M}_1$ and going over to the susceptibilities the expressions for the constants become after some algebra:

$$\bar{L}_0 \;=\; \frac{(\chi_1-\chi_2)\sinh\eta_o}{(1+\chi_2) - (1+\chi_1)\;\tanh^2\eta_o\;+\;(\chi_1-\chi_2)\;\sinh\eta_o\,\operatorname{arccot}(\sinh\eta_o)}, \tag{79}$$

$$\bar{L}_1 \;=\; -\,\frac{(\chi_1-\chi_2)\;\cosh^2\eta_o\;\sinh\eta_o}{2+\chi_1+\chi_2+(\chi_1-\chi_2)\;\cosh^2\eta_o\;\big(1-\sinh\eta_o\,\operatorname{arccot}(\sinh\eta_o)\big)}, \tag{80}$$

$$\bar{M}_0 \;=\; \frac{(1+\chi_1)\;\operatorname{sech}^2\eta_o}{(1+\chi_2) - (1+\chi_1)\;\tanh^2\eta_o\;+\;(\chi_1-\chi_2)\;\sinh\eta_o\,\operatorname{arccot}(\sinh\eta_o)}, \tag{81}$$

$$\bar{M}_1 \;=\; \frac{2(1+\chi_1)}{2+\chi_1+\chi_2+(\chi_1-\chi_2)\;\cosh^2\eta_o\;\big(1-\sinh\eta_o\,\operatorname{arccot}(\sinh\eta_o)\big)}. \tag{82}$$

The corresponding transformations are also given in the notebook OblateCoefficients.nb (Kraiger and Schnizer, 2011).

If both media are the same the external reaction potential must be zero. The internal potential must become the primary potential. Indeed, the limits of the four coefficients

$$\chi_2 \;\to\; \chi_1 : \quad \bar{L}_0 \to 0,\;\bar{L}_1 \to 0,\;\bar{M}_0 \to 1,\;\bar{M}_1 \to 1 \tag{83}$$

ensure this. In view of these results the reaction potentials, Φ_{r1} and Φ_{r2}, may be rewritten as:

$$\Phi_{1r} \;=\; \big(H_{0x}\;x\;+\;H_{0y}\;y\big)\bar{L}_1(g_1-g_2)\;+\;H_{0z}\;z\;\bar{L}_0(g_1-g_3), \tag{84}$$

$$\Phi_{2r}(x,y,z) \;=\; \big(H_{0x}\;x\;+\;H_{0y}\;y\big)(1-\bar{M}_1)\;\;+\;H_{0z}\;z\;(1-\bar{M}_0). \tag{85}$$

4.2 The reaction field in Cartesian coordinates

We want expressions for the potential which depend on x, y, z only. So $\sinh\eta$ must be replaced with a corresponding expression in Cartesian coordinates. From eqs.(58) to (60) one finds:

$$\sinh^2\eta \;=\; \frac{1}{2}\left(-1+\frac{r^2}{e_o^2}\pm\sqrt{\left(-1+\frac{r^2}{e_o^2}\right)^2+4\frac{z^2}{e_o^2}}\right).$$

Since the square root is larger than the preceeding polynomial it is obvious that only the plus sign applies. This is also confirmed by intense numerical studies. So we have:

$$\sinh\eta \;=\; \frac{1}{\sqrt{2}}\sqrt{-1+\frac{r^2}{e_o^2}+w_o(\mathbf{r},\mathbf{e}_z)} \;:=\; u_o(\mathbf{r},\mathbf{e}_z)/\sqrt{2}, \tag{86}$$

$$w_o(\mathbf{r},\mathbf{e}_z) \;=\; \sqrt{\left(-1+\frac{r^2}{e_o^2}\right)^2+4\frac{z^2}{e_o^2}} \;=\; \sqrt{\left(-1+\frac{r^2}{e_o^2}\right)^2+4\frac{(\mathbf{r}\cdot\mathbf{e}_z)^2}{e_o^2}}, \tag{87}$$

$$r^2 \;=\; x^2+y^2+z^2. \tag{88}$$

Inserting this expression for $\sinh\eta$ into eqs.(76) to (78) and inserting the resulting expressions for g_1, g_2, g_3

$$g_1 \;=\; \mathrm{acoth}(u_o(\mathbf{r},\mathbf{e}_z)/\sqrt{2}), \tag{89}$$

$$g_2 \;=\; \frac{\sqrt{2}\;u_o(\mathbf{r},\mathbf{e}_z)}{[u_o(\mathbf{r},\mathbf{e}_z)]^2+2}, \tag{90}$$

$$g_3 \;=\; \frac{\sqrt{2}}{u_o(\mathbf{r},\mathbf{e}_z)}. \tag{91}$$

into eq.(84) we get the final expression for the exterior potential as pure function of the Cartesian coordinates x, y, z:

$$\Phi_{r1}(x,y,z) \;=\; (H_{0x}\;x\;+H_{0y}\;y)\;\bar{L}_1\;(g_1-g_2)\;+\;H_{0z}\;z\;\bar{L}_0\;(g_1-g_3). \tag{92}$$

The interior potential, eq.(85), is already a pure function of the Cartesian coordinates.

4.3 Potential and field for an arbitrary direction of the spheroidal symmetry axis

For applications it is necessary to consider spheroids whose symmetry axis has an arbitrary direction. The corresponding expressions for the potential will be derived from those given in eqs.(92) and (85). These are rewritten in a way suggesting a general form:

$$\begin{aligned}\Phi_{r1}(x,y,z) &= (\mathbf{H}_{0\perp}\cdot\mathbf{r}_\perp)\;\bar{L}_1\;(g_1-g_2)\;+\;(\mathbf{H}_{0\parallel}\cdot\mathbf{r}_\parallel)\;\bar{L}_0\;(g_1-g_3),\\ \Phi_{r2}(x,y,z) &= (\mathbf{H}_{0\perp}\cdot\mathbf{r}_\perp)\;(1-\bar{M}_1)\;1\;(\mathbf{H}_{0\parallel}\cdot\mathbf{r}_\parallel)(1-\bar{M}_0).\end{aligned} \tag{93}$$

The meaning of the subscripts $\perp$ and $\parallel$ has already been explained above before and in eq.(41). $\mathbf{n}$ is a unit vector giving the symmetry axis of the spheroid.

In w_o, eq.(87), only the variable z, the component of the position vector along the z-axis, i.e. the symmetry axis, must be replaced by $(\mathbf{n}\cdot\mathbf{r})$ giving:

$$\sinh\eta \;=\; \frac{1}{\sqrt{2}}\sqrt{-1+\frac{r^2}{e_o^2}+\bar{w}_o(\mathbf{r},\mathbf{n})} \;:=\; \bar{u}_o(\mathbf{r},\mathbf{n})/\sqrt{2}, \tag{94}$$

$$\bar{w}_o(\mathbf{r},\mathbf{n}) \;=\; \sqrt{\left(-1+\frac{r^2}{e_o^2}\right)^2+4\frac{(\mathbf{n}\cdot\mathbf{r})^2}{e_o^2}}. \tag{95}$$

The functions g_i, eqs.(89) to (91), remain the same except that $u_o(\mathbf{r},\mathbf{e}_z)$ and $w_o(\mathbf{r},\mathbf{e}_z)$ must be replaced with $\bar{u}_o(\mathbf{r},\mathbf{n})$ and $\bar{w}_o(\mathbf{r},\mathbf{n})$ giving the new functions $\bar{g}_i$:

$$\bar{g}_1 \;=\; \operatorname{acoth}(\bar{u}_o(\mathbf{r},\mathbf{n})/\sqrt{2}), \tag{96}$$

$$\bar{g}_2 \;=\; \frac{\sqrt{2}\;\bar{u}_o(\mathbf{r},\mathbf{n})}{[\bar{u}_o(\mathbf{r},\mathbf{n})]^2+2}, \tag{97}$$

$$\bar{g}_3 \;=\; \frac{\sqrt{2}}{\bar{u}_o(\mathbf{r},\mathbf{n})}. \tag{98}$$

Inserting all these new functions into eqs.(93) gives the potential for an oblate spheroid whose symmetry axis is given by the arbitrary unit vector $\mathbf{n}$:

$$\begin{aligned}\Phi_{r1}(x,y,z) \;&=\; (\mathbf{H}_0\cdot\mathbf{r})\;\bar{L}_1\;(\bar{g}_1-\bar{g}_2)\;+\\ &+\; (\mathbf{H}_0\cdot\mathbf{n})(\mathbf{n}\cdot\mathbf{r})\;[\bar{L}_0\;(\bar{g}_1-\bar{g}_3)\;-\;\bar{L}_1\;(\bar{g}_1-\bar{g}_2)],\end{aligned} \tag{99}$$

$$\Phi_{r2}(x,y,z) \;=\; (\mathbf{H}_0\cdot\mathbf{r})\;(1-\bar{M}_1)\;+\;(\mathbf{H}_0\cdot\mathbf{n})(\mathbf{n}\cdot\mathbf{r})\;[\bar{M}_1\;-\;\bar{M}_0]. \tag{100}$$

The evaluation of the magnetic field requires the gradients of the functions $\bar{g}_i$. These are done by symbolic computation. Since the resulting expressions consist again of polynomials and the square roots already occuring in the potential it is possible to find simpler expressions. These are again checked against the original gradients by symbolic computation. All these derivatives are proportional to the vector $\mathbf{r}_o$

$$\mathbf{r}_o \;:=\; \frac{\sqrt{2}}{e_o^2}\left(\mathbf{r}\;+\;2\mathbf{n}\;\frac{(\mathbf{n}\cdot\mathbf{r})}{(\bar{u}_o(\mathbf{r},\mathbf{n}))^2}\right). \tag{101}$$

$$\nabla\bar{g}_1-\nabla\bar{g}_2 \;=\; -\;\frac{\bar{u}_o(\mathbf{r},\mathbf{n})}{\bar{w}_o(\mathbf{r},\mathbf{n})}\;\frac{4}{[(\bar{u}_o(\mathbf{r},\mathbf{n}))^2+2]^2}\;\mathbf{r}_o, \tag{102}$$

$$\nabla\bar{g}_1-\nabla\bar{g}_3 \;=\; \frac{2}{[2+(\bar{u}_o(\mathbf{r},\mathbf{n}))^2]\;\bar{u}_o(\mathbf{r},\mathbf{n})\;\bar{w}_o(\mathbf{r},\mathbf{n})}\;\mathbf{r}_o. \tag{103}$$

The corresponding checks are contained in the notebook OblatePotDerivatives.nb (Kraiger and Schnizer, 2011).

The vector $\mathbf{r}_o$ and all the gradients listed above are well-defined and real in the exterior of the oblate spheroid, where $\eta \geq \eta_o$; which is equivalent with the condition (107) in Cartesian coordinates. In fact, a more detailed analysis shows that on the interface:

$$\bar{u}_o(\mathbf{r},\mathbf{n}) \;=\; \sqrt{2}\;\sinh\eta_o, \tag{104}$$

$$\bar{w}_o(\mathbf{r},\mathbf{n}) \;=\; \sqrt{z^4/\left(e_o\;\sinh(\eta_o)\right)^4\;+\;2z^2/e_o^2\;+\;\sinh^4\eta_o} \tag{105}$$

$$\sinh^2\eta_o \leq \bar{w}_o(\mathbf{r},\mathbf{n}) \leq \cosh^2\eta_o. \tag{106}$$

In the exterior of the spheroid $\bar{u}_o(\mathbf{r},\mathbf{n})$, $\bar{w}_o(\mathbf{r},\mathbf{n})$ respectively are always larger than $\sqrt{2}\ \sinh\eta_o$, $\sinh^2\eta_o$ respectively. For a = 1, c = 2, ($e_o = \sqrt{3}$) one finds $\sqrt{2}\ \sinh\eta_o = \sqrt{2/3} = 0.816...$; $1/3 \leq \bar{w}_o(\mathbf{r},\mathbf{n}) \leq 4/3$.

4.4 Final formulas for the field

So the final formulas for the reaction field excited in an arbitray homogeneous primary field $\mathbf{H}_0$ by an oblate spheroid with arbitrary symmetry axis given by a unit vector $\mathbf{n}$ is in the exterior:

$$\frac{r^2-(\mathbf{n}\cdot\mathbf{r})^2}{a_o^2}+\frac{(\mathbf{n}\cdot\mathbf{r})^2}{c_o^2}\geq 1\ : \tag{107}$$

$$\begin{aligned}\mathbf{H}_{r1}(x,y,z) \;=\; & -\mathbf{H}_0\ \bar{L}_1\ (\bar{g}_1-\bar{g}_2)\ -\ \mathbf{n}(\mathbf{H}_0\cdot\mathbf{n})[\bar{L}_0\ (\bar{g}_1-\bar{g}_3)\ -\ \bar{L}_1\ (\bar{g}_1-\bar{g}_2)] \\ & +\mathbf{r}_o\ (\mathbf{H}_0\cdot\mathbf{r})\ \bar{L}_1\ \frac{\bar{u}_o(\mathbf{r},\mathbf{n})}{\bar{w}_o(\mathbf{r},\mathbf{n})}\ \frac{4}{[2+(\bar{u}_o(\mathbf{r},\mathbf{n}))^2]^2} \\ & -\mathbf{r}_o\ (\mathbf{H}_0\cdot\mathbf{n})(\mathbf{r}\cdot\mathbf{n})\ \bar{L}_0\ \frac{2}{[2+(\bar{u}_o(\mathbf{r},\mathbf{n}))^2]\ \bar{u}_o(\mathbf{r},\mathbf{n})\ \bar{w}_o(\mathbf{r},\mathbf{n})} \\ & -\mathbf{r}_o\ (\mathbf{H}_0\cdot\mathbf{n})(\mathbf{r}\cdot\mathbf{n})\ \bar{L}_1\ \frac{4\ \bar{u}_o(\mathbf{r},\mathbf{n})}{\bar{w}_o(\mathbf{r},\mathbf{n})\ [(\bar{u}_o(\mathbf{r},\mathbf{n}))^2+2]^2};\end{aligned} \tag{108}$$

and in the interior:

$$\frac{r^2-(\mathbf{n}\cdot\mathbf{r})^2}{a^2}+\frac{(\mathbf{n}\cdot\mathbf{r})^2}{c^2}\leq 1\ :$$

$$\mathbf{H}_{r2}(x,y,z) \;=\; \mathbf{H}_0\ (1-\bar{M}_1)\ +\ \mathbf{n}\ (\mathbf{H}_0\cdot\mathbf{n})\ [\bar{M}_1\ -\ \bar{M}_0]. \tag{109}$$

4.5 Concluding remarks for the field of an oblate spheroid

An oblate spheroid is inserted into an external homogeneous magnetic field $\mathbf{H}_0$ of arbitrary direction. Its permeability is $\mu_2 = \mu_0(1+\chi_2)$; while that of the surrounding medium is $\mu_1 = \mu_0(1+\chi_1)$. The spheroid has semi-axes $a_o, a_o, c_o,\ c_o < a_o$; these determine the excentricy e_o and the quasi-radial parameter η_o, eqs.(61) and (62). These in turn determine the coefficients $\bar{L}_0, \bar{L}_1, \bar{M}_0, \bar{M}_1$, eqs.(79) to (82). The spheroid's symmetry axis is the arbitrary unit vector $\mathbf{n}$. The reaction field due to the presence of the spheroid in the external field is given in Cartesian coordinates, $\mathbf{r} = (x,y,z)$, by eq.(108) in the exterior, by eq.(109) in the interior. The functions $\bar{g}_1, \bar{g}_2, \bar{g}_3$, eqs.(96) to (98), depend on the functions $\bar{u}_o(\mathbf{r},\mathbf{n})$ and $\bar{w}_o(\mathbf{r},\mathbf{n})$, eqs.(94) and (95). The needed gradients of the $\bar{g}_i$ are given in eqs.(102) and (103). Eqs.(108) and eq.(109) are for a spheroid, whose centre is at the origin. If the centre is at the point $\mathbf{r}_0 = (x_0, y_0, z_0)$ then the vector $\mathbf{r}$ must replaced simply with $\mathbf{r} - \mathbf{r}_0$.

5 Application: modelling trabecular bone

5.1 Introduction

Generally, in magnetic resonance experiments disturbances of the homogeneous main magnetic field have an essential impact on the formation of the resonance signal. In principle magnetic inhomogeneities can be classified with respect to their origin and strength, and their influence on the formation of the signal decay (Yablonksy and Haacke, 1994). Especially in MR-Osteodensitometry insights on the microarchitectural status of cancellous bone can be gained (Majumdar and Genant,1992; Wehrli *et al.*, 2006). In the space of spongy bone the relaxation properties of bone marrow are changed due to the susceptibility effects induced by the discontinuities of the magnetic susceptibility across the surface of the network of branching bone spicules (Davis *et al.*, 1986). In several studies direct relations between the effective transversal relaxation time T_2^*, a measure sensitive to field disturbances, and bone mineral density (BMD) (Grampp *et al.*, 1995; Link *et al.*, 1996; Arokoski *et al.*, 2002) and as well mechanical competence of trabecular bone (Chung *et al.*, 1993; Brismar *et al.*, 1997; Beuf *et al.*, 2001) were reported.

The resonance signal decay in a gradient echo MR experiment obeys, in case of these inhomogeneities being of Lorentzian characteristics, the following empirical expression:

$$S(T_E) \propto e^{-R_2^* T_E} \quad \text{with} \quad R_2^* = 1/T_2 + R_2' \,, \tag{110}$$

with T_2 giving the intrinsic transversal relaxation time and T_E the echo time. The quantity R_2' accounts for the additional contribution, originating from the local field inhomogeneities, to the effective transversal relaxation rate $R_2^* = 1/T_2^*$. Further, $R_2' \approx \gamma \Delta B$ with ΔB representing the field variation and γ the gyromagnetic ratio.

Computer simulations modelling the magnetic field distortion make it possible to gain insight into the interrelationship between the temporal characteristics of the resonance signal and the histomorphometrical parameters of the bone lattice. Hence interactions of morphometric quantities such as intertrabecular distance, trabecular thickness, bone volume fraction and the induced line broadening of the resonance spectra can be studied, as has been shown in (Kraiger, 2012) for situations of trabecular microcracks in a simplified model of vertebrae.

5.2 Simulation

A two-compartment model, consisting of bone marrow and the mineralized bone, was applied evaluating the magnetic field distribution. For the simulation of architectures made up by plate-like trabeculae, as they can be found in the epiphysis of long bones like the femur, oblate spheroids were used. Hence, in a three-dimensional unit cell representing the volume of interest (VOI) ellipsoids were arranged appropriately to model the known trabecular microstructure (Hildebrand *et al.*, 1999).

Following the approach described by (Bakker *et al.*, 1992), the reaction fields induced by the susceptibility difference between the ellipsoids (trabeculae) and the background (bone marrow) were computed at first. Subsequently the time

course of the resonance signal was computed applying a Fourier Transformation of the spatial magnetic field distribution with respect to time (Ford *et al.*, 1993).

In a homogeneous magnetic field the precession frequency of spins is determined through the magnetic induction $\mathbf{B}$. Now introducing a sample with a different susceptibility - in the current experiment trabecular bone (χ_2) is surrounded by bone marrow (χ_1) - the resulting magnetic induction B_z can be generally written as:

$$B_z = \mu \left(H_{0z} + M_z \left(\mathbf{r} \right) \right) = \mu_0 (1 + \chi) \left(H_{0z} + M_z \left(\mathbf{r} \right) \right), \tag{111}$$

with M_z characterising the induced reaction field. Herein the units are given in the MKS-system, and susceptibility units are per unit volume.

Since the transversal magnetization decay of mineralized bone is several magnitudes faster comparing to bone marrow, the received resonance signal in MR-Osteodensitometry is governed by the magnetization arising within the marrow. Hence M_z corresponds to the computed reaction field $\Delta H_{r1,z}$ caused by the difference in magnetic property between bone and marrow.

Within the unit cell the distribution of the reaction field originating from the n ellipsoids was determined as the sum of all individual contributions H_{r1i}:

$$\Delta H_{r1,z} \left(\mathbf{r} \right) = \sum_{i=1}^{n} H_{r1i} \left(\mathbf{r} \right). \tag{112}$$

Interactions between the trabeculae have been neglected. This assumption is valid, since such interactions include susceptibility effects of the second order, which will give rise to field contributions of $\mathbf{H}_0 \left(\Delta\chi \right)^2$, or $\approx \mathbf{H}_0 \cdot 10^{-12}$.

In a simple MR experiment, RF excitation followed by an acquisition period, the signal of the free induction decay (FID) can be written as:

$$S(t) = \text{const} \int\limits_{VOI} d^3\mathbf{r} \; e^{-i\omega(\mathbf{r})t} \; e^{-t/T_2}; \tag{113}$$

with $\omega(\mathbf{r}) = \gamma B_z(\mathbf{r})$ it follows:

$$S(t) = \text{const} \int\limits_{VOI} d^3\mathbf{r} \; e^{-i\gamma B_z(\mathbf{r})t} \; e^{-t/T_2}. \tag{114}$$

Applying (111) again, the following expression in H_z can be found:

$$S(t) = \text{const} \int\limits_{VOI} d^3\mathbf{r} \; e^{-i\gamma t \; \mu_0(1+\chi_1)(H_{0z}+\Delta H_{r1,z}(\mathbf{r}))} \; e^{-t/T_2}. \tag{115}$$

This integral must be extended over the entire unit cell enclosing all ellipsoids.

In order to compare the simulation results with commonly acquired MR magnitude images $S(t)$ has to be further processed. From eq.(115) it is clear, that except for the dissipative relaxation phenomenon e^{-t/T_2} the expressions are purely oscillatory in H_{0z}. Hence, the essential decay for the analysis of the signal course can be expressed as:

$$|S(t)| = \text{const} \int\limits_{VOI} d^3\mathbf{r} \; e^{-i\gamma t \; \mu_0(1+\chi_1)\Delta H_{r1,z}(\mathbf{r})}. \tag{116}$$

$\Delta H_{r1,z}(\mathbf{r})$ can be computed according to (112) as the sum over all the reactions fields of the individual ellipsoids, where $\mu_0(1+\chi)$ describes the magnetic permeability at the location $\mathbf{r}$.

5.2.1 Algorithm

Utilizing the expression developed for the reaction field of an oblate ellipsoid eq.(108) the simulations were implemented in *Mathematica* (Wolfram Research, Inc.). As input parameters the spacing of the trabeculae in x-, y- and z-direction, the dimensions of the ellipsoids and the position of the symmetry axis with respect to the z-axis of the coordinate system had to be defined. Further, the susceptibilities of the bones, the background and the orientation of the applied homogenous main magnetic field had to be set. The program computed the field distribution of the z-component of the reaction fields in the sense of a histogram and generated the MR signal curve according to (116). The obtained signal was subsequently processed within a fitting-procedure yielding the relaxation constant R_2'.

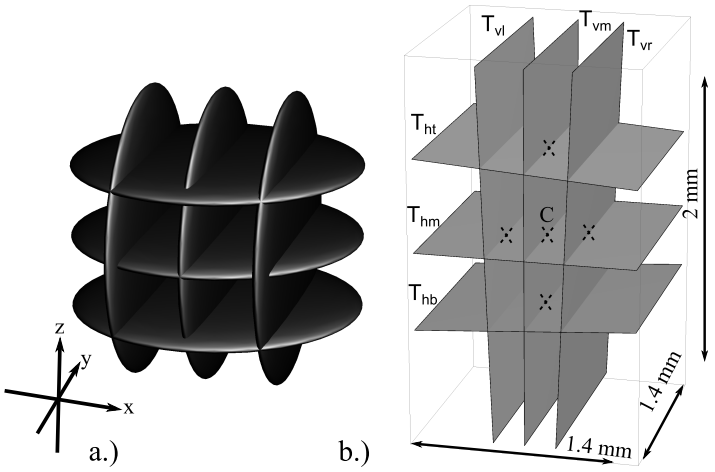

Figure 1: a.) Schematic depiction of six oblate ellipsoids forming the three-dimensional plate-like microstructure of Model I; b.) Detailed view of the applied unit cell; dimensions are given in *mm*. The centres of the ellipsoids are indicated by crosses, the subscripts *v, h* are denote the horizontal and vertical flat ellipses representing the trabeculae in the array; *C* indicates the origin.

5.2.2 T_2' Data fitting

From the simulated signal curves the relaxation time was estimated assuming a Gaussian signal model (Selby *et al.*, 1996; Fransson *et al.*, 1998). The signal intensities computed at the echo times ranging from 0 to 50 ms (eq.(116)), 2.5 ms increment, were used to generate a single T_2' value by means of a non linear least-squares-approximation to a three parameter fit function:

$$S(t) = A + B\ e^{-t^2/\left(2T_2'^2\right)}\ . \tag{117}$$

The fitting model is equivalent to a bi-Gaussian function with one term having a decay constant greater than the maximum T_E (50 ms). A high value of the ratio A/B corresponds to a decay that deviates significantly from a single Gaussian (Newitt *et al.*, 1996; Fransson *et al.*, 1998).

5.2.3 Model: plate-like trabecular structure

The effect of the loss of bone mass within a three-dimensional plate-like trabecular model was analysed using oblate ellipsoids. Hence, stepwise decreasing of the bone volume fraction $\varsigma = BV/TV$, bone volume (BV)/total volume (TV), was performed. In accordance with the findings of (Hildebrand *et al.*, 1999), ς values ranging from 0.530–0.406 were investigated. The bone remodelling was simulated as a simultaneous decrease of the thickness of the horizontal and vertical ellipsoids by 12.5 μm.

The configuration of the 3D unit cell and the parameter settings are shown in Figure 1, Tables 1 and 2.

Parameters				
Trabecula	*Vector* $\mathbf{n}$ *(x,y,z)*		*Center T (x,y,z)*	
	$\mathbf{n}_v$	$\mathbf{n}_h$	T_v	T_h
left/**t**op	$\sin 10^\circ, 0, \cos 10^\circ$	$0, \sin 95^\circ, \cos 95^\circ$	-400,0,0	0,0,-700
middle	$1, 0, 0$	$0, 0, 1$	$0, 0, 0$	$0, 0, 0$
right/**b**ottom	$\sin 15^\circ, 0, \cos 15^\circ$	$0, \sin 95^\circ, \cos 95^\circ$	400,0,0	0,0,700

Table 1: Parameters of the oblate ellipsoids utilized in Model I. Units of the centres are given in μm. The susceptibility of the trabecular bone and the bone marrow were set to $\chi_1 = -0.62 \times 4\pi \times 10^{-6}$ and $\chi_2 = -0.9 \times 4\pi \times 10^{-6}$, respectively (Hopkins and Wehrli, 1997). A main magnetic induction of $B_{0z} = 3$ T, $\alpha = 5^\circ$ and $\beta = 0^\circ$ was applied.

5.2.4 Simulating bone loss

In this subsection the results of the analysis studying the effect of loss of bone mass on the field distribution and the resulting relaxation constant T_2' are presented. The resulting histograms are reflecting the impact of decreasing ς on the field distribution of the reaction fields, see Figure 2. Depending on the fraction the reaction fields varried approximately between -0.6 and -0.05 A/m. As a consequence of the bone loss the field distribution became more homogeneous,

	Dimensions	
ellipsoids	$a/b_{v,h}$	3000/100 μm
unit cell	volume	3.92 mm^3
initial BV/TV	ς_0	0.482

Table 2: Dimensions of the ellipsoids, the unit cells and the initial bone volume fractions BV/TV.

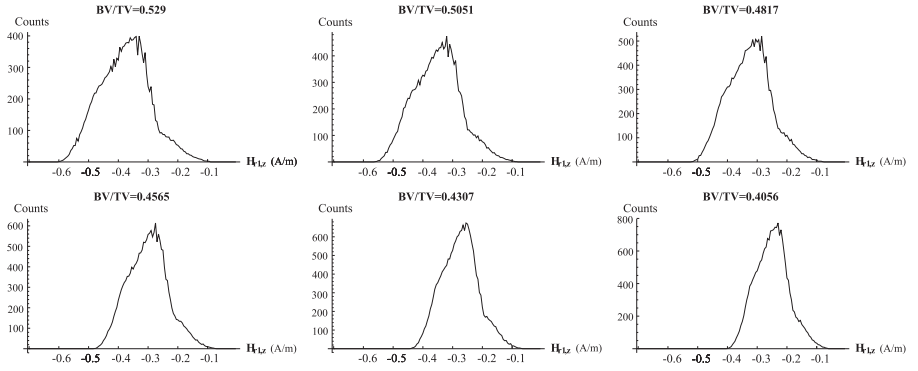

Figure 2: Resulting field distributions of the reaction field $H_{r1,z}$ induced by the susceptibility effect between bone and bone marrow. The fields were computed within the entire volume of Model I as a function of ς. A main magnetic field $B_{0z} = 3$ T, respective $H_{0z} = 2.38732 \cdot 10^6$ A/m with $\alpha = 5°$ and β parallel z-axes, and values of $\chi_1 = -0.62 \cdot 4 \cdot \pi \cdot 10^{-6}$ and $\chi_2 = -0.9 \cdot 4 \cdot \pi \cdot 10^{-6}$ were applied.

hence the broadness of the histogram narrowed, whereby its maxima was shifted in the direction of a more positive field strength.

The simulated signal curves as a function of ς are presented in Figure 3 together with the estimated relaxation times. The estimated parameters of the least-squares approximation are given in Table 3. During the decrease of ς

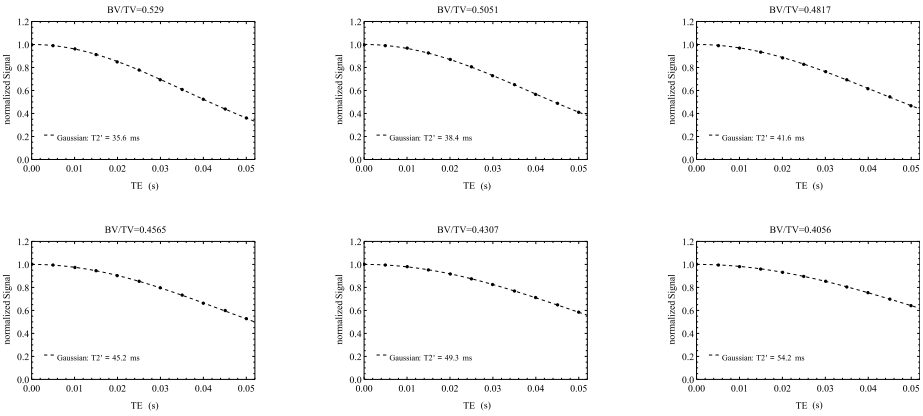

Figure 3: Simulated impact of the computed reaction field $H_{r1,z}$ on the MR signal decay. The signals are normalized to the values at the first echo time T_E and presented for various bone volume fractions ς. Markers are indicating the computed signal values at T_E, whereby the dashed curve was obtained using the estimated parameters of the Gaussian fit-function.

the applied Gaussian signal model responded with a moderate increase of T_2'. Further, the Gaussian approach exhibited an almost linear relation between the loss of bone mass and the increase of T_2', as can be concluded from Table 3 .

BV/TV	A_{gau}	B_{gau}	T_2' (ms)	RMSE
0.530	-0.021	1.021	36.10	$0.12 \cdot 10^{-3}$
0.505	-0.029	1.030	38.86	$0.10 \cdot 10^{-3}$
0.482	-0.035	1.035	42.12	$0.07 \cdot 10^{-3}$
0.457	-0.035	1.035	45.78	$0.05 \cdot 10^{-3}$
0.431	-0.038	1.038	49.99	$0.03 \cdot 10^{-3}$
0.406	-0.035	1.035	54.88	$0.02 \cdot 10^{-3}$

Table 3: Resulting parameter estimates of the non-linear least-squares approximation of the simulated signal decay to a Gaussian function. The approximations were performed for various ς.

5.3 Discussion

The novel analytical solutions of the three-dimensional Laplacian potential problem of spheroids were successfully applied in the area of MR-Osteodensitometry. Especially coordinate transformations became unnecessary, thus simplifying the modelling of arbitrary orientated trabecular bones in an arbitrary orientated main magnetic field.

To the authors best knowledge for the first time oblate ellipsoids were used to mimic the field effects of plate-like structures more realistically. Such structures made it possible to study the effects of bone mass loss in a basic model of oseous bone. In principle there are no restrictions concerning the amount and orientation of the used oblate spheroids, hence even complex architectures are accessible for modelling.

In the case of bone disorders such as osteoporosis annual changes of the bone mass between 2–5 % were reported (Harris and Dawson-Hughes,1992; Davis *et al.*, 1991). Applying the presented novel analytical field expressions, such realistic alterations in conjunction with their effects on the MR relaxation parameter T_2' can be studied. In the current simulations minor alterations of $\Delta\varsigma = 0.025$ were successfully modelled, yielding variations of the MR relaxation parameter T_2' in a measurable range of ms. The presented results are qualitatively comparable with previously reported studies, whereby either a different size of the volume of interest or different trabecular elements, rod-like structures, were utilized (Selby *et al.*, 1996; Chung *et al.*, 1996).

In general, the use of the analytical field expression of the prolate case enables the investigation of induced field distortions in the surrounding of the trabecular microcracks. This has been studied in a second application described in the report given by (Kraiger and Schnizer, 2011). In an additional study using a more realistic 3D bone model the variations of the reaction fields along the progression of pathological bone remodelling are under investigation. The results of the ongoing study will be published elsewhere.

6 Conclusions

1. Expressions for the potential and field of a prolate spheroid in a homogeneous external field of arbitrary direction have been derived in prolate spheroidal coordinates. These expressions have been transformed to

Cartesian coordinates. The resulting expressions have been generalized to an arbitrary direction of the symmetry axis while the external field axis may still have another arbitrary direction.

2. The same has been done for an oblate spheroid with arbitrary symmetry axis and an other arbitrary field axis.

3. Since the magnetic susceptibilites of biological tissues are small (volume susceptibility $\approx -10^{-6}$) (Schenck,1996) it is easy to construct models of trabecular bone structures by arrays of spheroids as described in the previous item. The total magnetic induction is that of the primary field plus that of all the spheroids in the array to a very good approximation which disregards the small magnetic interaction of the spheroids among themselves.

4. This modelling is particularly easy since all field dependences may be expressed in the same general Cartesian coordinate system.

5. As an example of the method the following configuration is treated: Oblate spheroids are used in a 3D model to study the impact of trabecular bone loss on the MR signal decay characteristic.

6. In the present work just one application of the analytical expressions, the modelling of bone disorders in the area of MR-Osteodensitometry, was given. For example in the field of functional MRI the devoloped toolbox eases the analysis of the BOLD (blood oxygenation level-dependent) contrast, where induced reaction fields in the surrounding of vascular networks are of great interest (Ogawa *et al.*, 1990). A fast and precise computation of the magnetic distortion is essential for improving the precision of the temperature determination in techniques using the proton resonance frequency (PRF) shift method (Hindmann, 1966; Rieke and Pauly, 2008). Temperature mapping in the vicinity of the needle electrode is a crucial determinant of MRI guided interventional radiofrequency ablations (Boss *et al.*, 2005). Further, in the field of metabolism studies using NMR spectroscopy (MRS) the expressions can be used in order to model specific cells introduced in solutes differing in magnetic susceptibility (Kuchel, 1983).

7. The authors believe that the novel formulation of solutions depending solely on the Cartesian coordinates will facilitate the modelling of countless magnetostatic problems.

Not added in proof:

A very concise compilation of the formulas of this paper together with some new formulas for the coefficients $L_0, L_1, ..., \bar{M}_1$ have been given in Kraiger and Schnizer (2112).

References

Arokoski, M.H., Arokoski, J.P., Vainio, P., Niemitukia, L.H., Kroeger, H. and Jurvelin, J.S. (2002), "Comparison of DXA and MRI methods for interpreting femoral neck bone mineral density", *Journal of Clinical Densitometry*, vol.5, pp. 289-296.

Bakker, C.J.C., Bhagwandien, R., Moerland, M.A. and Fuderer, M. (1992), "Susceptibility artifacts in 2D FT spin-echo and gradientecho imaging: the cylinder model revisted", *Magnetic Resonance Imaging*, vol.11, pp. 539-548.

Beuf, O., Newitt, D.C., Mosekilde, L. and Majumdar, S. (2001), "Trabecular structure assessment in lumbar vertebrae specimens using quantitative magnetic resonance imaging and relationship with mechanical competence", *Journal of Bone and Mineral Research* vol.16, pp.1511-1519.

Boss, A., Graf, H., Mülller-Bierl, B., Clasen, S., Schmidt, D., Pereira, P.L. and Schick, F. (2005), "Magnetic susceptibility effects on the accuracy of MR temperature monitoring by the proton resonance frequency method", *Journal of Magnetic Resonance Imaging*, vol.22, pp. 813-820.

Brismar, T.B., Hindmarsh, T. and Ringertz, H. (1997), "Experimental correlation between T2* and ultimate compressive strength in lumbar porcine vertebrae", *Academic Radiology*, vol.4, pp. 426-430.

Chung, H-W., Hwang, S.N., Yeung, H.N. and Wehrli, F.W. (1996), "Mapping of the magnetic-field distribution in cancellous bone", *Journal of Magnetic Resonance, Series B*, vol.113, pp.172-176

Chung, H., Wehrli, F.W., Williams, J.L. and Kugelmass, S.D. (1993), "Relationship between NMR transverse relaxation, trabecular bone architecture and strength", *Proceedings of the National Academy of Sciences of the United States of America*, vol.90, pp.10250-10254.

Davis, C.A., Genant, H.K. and Dunham, J.S. (1986), "The effects of bone on proton NMR relaxation times of surrounding liquids", *Investigative Radiology*, vol.21, pp.472-477.

Davis, J.W., Ross, P.D., Wasnich, R.D., MacLean, C.J. and Vogel, J.M. (1991), "Long-term precision of bone loss rate measurements among postmenopausal women", *Calcified Tissue International*, vol.48, pp.311-318.

Ford, J.C., Wehrli, F.W. and Chung, H-W. (1993), "Magnetic field distribution in models of trabecular bone", *Magnetic Resonance in Medicine* vol.30, pp.373-379.

Fransson, A., Grampp, S. and Imhof, H.: (1999), "Effects of trabecular bone on marrow relaxation in the tibia", *Magnetic Resonance Imaging*, vol. 17, pp.69-82.

Grampp, S., Majumdar, S., Jergas, M., Lang, P., Gies, A. and Genant, H.K. (1995), "MRI of bone marrow in the distal radius: in vivo precision of effective transverse relaxation times", *European Radiology*, vol.5, pp.43-48.

Harris, S. and Dawson-Hughes, B. (1992), "Rates of change in bone mineral density of the spine, heel, femoral neck, and radius in healthy postmenopausal women", *Bone and Mineral*, vol.17, pp.87-95.

Hildebrand, T., Laib, A., Müller, R., Dequeker, J. and Rüegsegger, P. (1999), "Direct three-dimensional morphometric analysis of human cancellous bone: microstructural data from spine, femur, iliac crest, and calcaneus", *Journal of Bone and Mineral Research* vol.14, pp.1167-1174.

Hindman, J.C. (1966), "Proton resonance shift of water in gas and liquid states", *Journal of Chemical Physics*, vol.44, pp.4582-4592.

Hopkins, J.A. and Wehrli, F.W. (1997),"Magnetic susceptibility measurement of insoluble solids by magnetic susceptibility of bone", *Magnetic Resonance in Medicine*, vol.37, pp.494-500.

Kraiger, M. (2012), "Methodische Aspekte der quantitativen Magnetresonanztomographie für endogene Biomarker auf dem Gebiet der muskuloskeletalen Bildgebung", Doctoral Dissertation,Technische Universität Graz, Austria.

Kraiger, M., and Schnizer, B. (2011), "Reaction fields of homogeneous magnetic spheroids of arbitrary direction in a homogeneous magnetic field. A toolbox for MRI and MRS of heterogeneous tissue", Report 2011-021CorRev (revised October 2012, corrected 2014-01-14); *Mathematica* notebooks. http://itp.tugraz.at/∼schnizer/MedicalPhysics/.

Kraiger, M., and Schnizer, B. (2012), "Potential of spheroids in a homogeneous magnetic field in Cartesian coordinates", Proc. IGTE'12, 15 th International IGTE Symposium on Numerical Field Calculations in Electrical Engineering, Graz, Austria, 16 to 19 September 2012, pp. 310-314, ISBN 978-3-85125-258-3.

Kuchel, Ph.W. (1983),"Red cell metabolism: studies using NMR spectroscopy", *Proceedings of Australian Biochemistry Society*, vol.15, pp.P5-P6.

Kuchel, Ph. W. and Bulliman, Br.T. (1989), "Perturbation of Homogeneous Magnetic Fields By Isolated Single and Confocal Spheroids. Implications for NMR Spectroscopy of Cells", *NMR in Biomedicine*, vol.2, pp.151-160.

Link, T.M. , Lin, J.C., Newitt, D., Meier, N., Waldt, S. and Majumdar, S. (1998), "Computergestützte Strukturanalyse des trabekulären Knochens in der Osteoporosediagnostik", *Der Radiologe*, vol.38, pp.853-859.

Majumdar, S. and Genant, H.K. (1992), "In vivo relationship between marrow T2* and trabecular bone density determined with a chemical shiftselective asymmetric spin-echo sequence", *Journal of Magnetic Resonance Imaging*, vol. 2, pp.209-219.

Moon, P. and Spencer, D.E. (1988), *Field Theory Handbook. Including Coordinate Systems, Differential Equations and their Solutions*, Springer, Berlin.

Newitt, D.C., Majumdar, S., Jergas, M.D. and Genant, H. (1996), "Decay characteristics of bone marrow in the presence of a trabecular bone network: In vitro and In vivo studies showing a departure from monoexponential behavior", *Magnetic Resonance in Medicine* vol.35, pp. 921-927.

Ogawa, S., Lee, T.M., Kay, A.R. and Tank, D.W. (1990), "Brain magnetic resonance imaging with contrast dependent on blood oxygenation", *Proceedings of the National Academy of Sciences of the United States of America*, vol.87, pp.9868-9872.

Rieke, V., and Pauly, K.B. (2008), "MR thermometry", *Journal of Magnetic Resonance Imaging*, vol.27, pp.376-390.

Schenck, J.F. (1996), "The role of magnetic susceptibility in magnetic res-

onance imaging: MRI magnetic compatibility of the first and second kinds", *Medical Physics* vol.23, pp. 816-850.

Selby, K., Majumdar, S., Newitt, D. and Genant, H.K. (1996), "Investigation of MR decay rates in microphantom models of trabecular bone", *Journal of Magnetic Resonance Imaging*, vol.6 ,pp.549-559.

Wehrli, F.W., Song, H.K., Saha, P.K. and Wright, A.C. (2006), "Quantitative MRI of the assessment of bone structure and function", *NMR in Biomedicine*, vol.19,pp. 731-764.

Yablonskiy, D.A. and Haacke, E.M. (1994),"Theory of NMR signal behavior in magnetically inhomogeneous tissues: the static dephasing regime", *Magnetic Resonance in Medicine*, vol.32, pp. 749-763.

About the authors

B. Schnizer is a Professor Emeritus at the Faculty of Physics, University of Technology Graz, where he teaches courses on analytical methods in applied theoretical physics and on symbolic computations (Mathematica). Currently, he is mainly involved in research on analytical field computations (Green's functions) in simple models of counters and accelerator magnets.

M. Kraiger received the diploma degree in biomedical engineering from the University of Technology Graz, Austria; and his Dr. techn. working there at the Institute of Medical Engineering. Afterwards he joined the PET-Center Group at the Helmholtz-Zentrum Dresden-Rossendorf, where he was responsible for the magnetic resonance imaging of the PET-MRI system. His research was focused on quantitative perfusion imaging and development of MRI perfusion measurements. Currently he is again working at the Institute of Medical Engineering of TU Graz in the field of quantitative MRI. He can be reached under m.kraiger@tugraz.at.